D-Trehalose/D-maltose-binding protein from the hyperthermophilic archaeon Thermococcus litoralis: The binding of trehalose and maltose results in different protein conformational s...

ARTICLE *in* PROTEINS STRUCTURE FUNCTION AND BIOINFORMATICS · JUNE 2006

Impact Factor: 2.63 · DOI: 10.1002/prot.20952 · Source: PubMed

9 AUTHORS, INCLUDING:

Petr Herman
Charles University in Prague
85 PUBLICATIONS **1,517** CITATIONS
SEE PROFILE

Anna Marabotti
Università degli Studi di Salerno
81 PUBLICATIONS **841** CITATIONS
SEE PROFILE

Fabio Tanfani
Università Politecnica delle Marche
128 PUBLICATIONS **2,249** CITATIONS
SEE PROFILE

Mosè Rossi
Italian National Research Council
305 PUBLICATIONS **5,487** CITATIONS
SEE PROFILE

PROTEINS: Structure, Function, and Bioinformatics 63:754–767 (2006)

D-Trehalose/D-Maltose-Binding Protein From the Hyperthermophilic Archaeon *Thermococcus litoralis*: The Binding of Trehalose and Maltose Results in Different Protein Conformational States

Petr Herman,[1]* Maria Staiano,[2] Anna Marabotti,[3,4] Antonio Varriale,[2] Andrea Scirè,[5] Fabio Tanfani,[5] Jaroslav Vecer,[1] Mose' Rossi,[2] and Sabato D'Auria[2]*

[1]*Faculty of Mathematics and Physics, Institute of Physics, Charles University, Prague, Czech Republic*
[2]*Institute of Protein Biochemistry, CNR, Naples, Italy*
[3]*Laboratory of Bioinformatics, Institute of Food Science, CNR, Avellino, Italy*
[4]*Interdepartmental Research Center for Computational and Biotechnological Sciences, Second University of Naples, Napoli, Italy*
[5]*Institute of Biochemistry, Polytechnical University of Marche, Ancona, Italy*

ABSTRACT **In this work, we used fluorescence spectroscopy, molecular dynamics simulation, and Fourier transform infrared spectroscopy for investigating the effect of trehalose binding and maltose binding on the structural properties and the physical parameters of the recombinant D-trehalose/D-maltose binding protein (TMBP) from the hyperthermophilic archaeon *Thermococcus litoralis*. The binding of the two sugars to TMBP was studied in the temperature range 20°–100°C. The results show that TMBP possesses remarkable temperature stability and its secondary structure does not melt up to 90°C. Although both the secondary structure itself and the sequence of melting events were not significantly affected by the sugar binding, the protein assumes different conformations with different physical properties depending whether maltose or trehalose is bound to the protein. At low and moderate temperatures, TMBP possesses a structure that is highly compact both in the absence and in the presence of two sugars. At about 90°C, the structure of the unliganded TMBP partially relaxes whereas both the TMBP/maltose and the TMBP/trehalose complexes remain in the compact state. In addition, Fourier transform infrared results show that the population of α-helices exposed to the solvent was smaller in the absence than in the presence of the two sugars. The spectroscopic results are supported by molecular dynamics simulations. Our data on dynamics and stability of TMBP can contribute to a better understanding of transport-related functions of TMBP and constitute ground for targeted modifications of this protein for potential biotechnological applications. Proteins 2006;63:754–767.**

Key words: trehalose/maltose-binding protein; periplasmic protein; biosensors; tryptophan fluorescence; FTIR; bidimensional infrared spectroscopy; molecular dynamics simulations

INTRODUCTION

The D-trehalose/D-maltose-binding protein (TMBP) is one component of the trehalose (Tre) and maltose (Mal) uptake system that is in the hyperthermophilic archaeon *Thermococcus litoralis* mediated by a protein-dependent ATP-binding cassette (ABC) transporter. High-affinity binding protein-dependent transporters were first discovered in gram-negative bacteria where the water-soluble substrate-binding proteins are located in the periplasmic space between the inner and outer membranes. Later, similar binding protein-dependent ABC transporters were also found in gram-positive bacteria,[1] thermophilic bacteria,[2,3] and archaea.[4–6]

TMBP from *T. litoralis* is a monomeric 48-kDa[4] two-domain macromolecule containing 12 tryptophan residues.[7] Because of high sensitivity of indole emission to local interactions and variations in microenvironment, tryptophan residues may be used with advantage as

Abbreviations: TMBP, D-trehalose/D-maltose-binding protein; TMBP/Mal, TMBP in the presence of 10 mM D-maltose; TMBP/Tre, TMBP in the presence of 10 mM D-trehalose; Mal, D-maltose; Tre, D-trehalose; OD, optical density; FTIR, Fourier transform infrared; Amide I′, Amide I band in a ^2H_2O medium; 2D-IR, bidimensional infrared spectroscopy; H-bonds, hydrogen bonds; MD, molecular dynamics; SV, Stern-Volmer, NATA, N-acetyltryptophanamide

Grant sponsor: NATO-CNR; Grant number: 218.2049; Grant sponsor: Ministry of Education, Youth and Sports of the Czech Republic; Grant number: MSM 0021620835; Grant sponsors: FIRB; Università Politecnica delle Marche (Ricerca di Ateneo); CRdC-ATIBB POR UE-Campania Mis. 3.16 activities; CNR Commessa Diagnostica avanzata ed alimentazione.

This work is dedicated to Prof. Winfried Boos, University of Konstanz, Germany, for his outstanding contribution to the microbiology and biochemistry of thermophilic organisms.

*Correspondence to: Petr Herman, Institute of Physics, Charles University, Ke Karlovu 5, 121 16 Prague, Czech Republic. E-mail: herman@karlov.mff.cuni.cz or Sabato D'Auria, Institute of Protein Biochemistry, CNR, Via P. Castellino, 111, 80131 Napoli, Italy. E-mail: s.dauria@ibp.cnr.it

Received 2 September 2005; Revised 12 November 2005; Accepted 19 December 2005

Published online 10 March 2006 in Wiley InterScience (www.interscience.wiley.com). DOI: 10.1002/prot.20952

intrinsic spectroscopic probes for monitoring of protein structural properties in solution.[8] Structural fluctuations perturbing Trp fluorescence characteristics may be related to local events near or involving the probe and its immediate environment, or to slower processes involving the entire protein structure, or both.

TMBP shares common structural motifs with several other sugar-binding proteins. These proteins consist of two globular domains connected by a hinge region made of two or three short polypeptide segments. The two domains are formed by noncontiguous polypeptide stretches and exhibit similar tertiary structure. The sugar-binding site is located in the deep cleft between the two domains and the binding is accompanied by a movement of the two lobes[9] as well as conformational changes in the hinge region.[10]

Ligand-binding proteins from protein-dependent ABC transport systems are good candidates for a design of highly specific fluorescence biosensors for small analytes.[11] The recombinant TMBP from *T. litoralis* is highly thermostable and binds both Tre and Mal with a K_d of 0.160 μM.[12] A sensor based on this biological recognition element would have excellent stability and shelf life. Because both Mal and Tre are composed of two glucose subunits, it is not so outrageous to envision targeted modifications of this protein that would result, e.g., in a fluorescent biosensor for diabetic patients. When planning future biotechnological applications involving modifications and/or labeling of proteins, detailed knowledge of their properties, stability, and structural configurations in a solution is of high importance.

In this work we investigate the effect of the Mal binding and Tre binding to TMBP on the configuration and thermal stability of TMBP by means of fluorescence spectroscopy and Fourier transform infrared (FTIR) spectroscopy. Experiments were done at temperatures between 20° and 100°C and conclusions were correlated with the results obtained from the molecular dynamics (MD) simulations experiments.

MATERIALS AND METHODS

Materials

D-maltose and D-trehalose were purchased from Sigma, deuterium oxide (99.9% ^2H_2O), ^2HCl, and NaO^2H were purchased from Aldrich. All other chemicals were commercial samples of the best available quality.

Purification of TMBP and Protein Concentration Determination

Twenty grams cell wet weight of the *Escherichia coli* cell pellet containing the expressed TMBP was resuspended in 50 mM Tris-HCl, pH 7.5, 500 mM NaCl (100 mL), ruptured by a French pressure cell at 16,000 psi, and centrifuged for 15 min at 19,000*g*. The supernatant was heated to 90°C for 20 min and centrifuged for 15 min at 19,000*g*. The supernatant was collected and dialyzed for 12 h against 10 mM Tris-HCl, pH 7.5 at 4°C. The solution was loaded onto a DEAE column previously equilibrated in 10 mM Tris-HCl, pH 7.5. After washing the column with 10 mM Tris-HCl, pH 7.5, TMBP was eluted by a NaCl gradient (0.0 M NaCl to 1.0 M NaCl). Centricon 30 concentrator (Amicon) was used to concentrate and to dialyze TMBP against 10 mm Tris-HCl, pH 7.5. The purified protein was treated with a streptomycin sulfate step and after that the protein solution was passed through a Blue A affinity column (Amersham) to obtain DNA-free TMBP. The purity of TMBP was verified by sodium dodecyl sulfate–polyacrylamide gel electrophoresis and absorption spectra.

The protein concentration was determined by the method of Bradford[13] with bovine serum albumin as standard on a double beam Cary 1E spectrophotometer (Varian, Mulgrade, Victoria, Australia).

Steady-State Fluorescence Spectroscopy

Steady-state fluorescence data were measured on the Fluoromax 3 spectrofluorometer (SPEX) equipped with a four-cell temperature-controlled sample holder. Trp fluorescence was excited at 295 nm with the slit width of 1 nm. Temperature of samples was measured directly in the cuvette by a thermocouple.

Time-Resolved Fluorescence Measurements

Frequency domain fluorescence experiments were performed on the K2 fluorometer (ISS, Urbana-Champaign) as described previously.[14] To selectively excite Trp residues, fluorescence was excited at 295 nm with a slit width of 5 nm. Protein emission was selected by a combination of a Zeiss UG1 and 345-nm cutoff filters that allowed for elimination of the elastic scatter and Raman bands of water near 335 nm. Samples were placed in a thermostatic holder connected to a water bath. Intensity decays were analyzed in terms of the multiexponential model:

$$I(t) = \sum_i \alpha_i \exp(-t/\tau_i) \quad (1)$$

where α_i are the preexponential factors, τ_i the decay times, and $\Sigma\alpha_i = 1.0$. For multicomponent decays, the fractional intensity f_i of each decay time is given by

$$f_i = \frac{\alpha_i \tau_i}{\sum_j \alpha_j \tau_j} \quad (2)$$

and the mean lifetime can be calculated as:

$$\bar{\tau} = \sum_i f_i \tau_i. \quad (3)$$

Fluorescence Quenching

Acrylamide quenching of the protein fluorescence was observed at the fluorescence maximum and analyzed by the Stern-Volmer equation:

$$F_0/F = 1 + K_{SV} \cdot [Q] = 1 + k_q \bar{\tau}_0 \cdot [Q] \quad (4)$$

where F and F_0 are the fluorescence intensities in the presence and in the absence of the quencher, respectively, $[Q]$ is a concentration of the quencher and τ_0 is a mean fluorescence lifetime in the absence of quencher. The

terms K_{sv} and k_q represent the Stern-Volmer and the bimolecular quenching constants, respectively.

Stern-Volmer Equation for Two Classes of Tryptophan Residues

When indicated, the quenching was analyzed using a model that assumes two classes of Trps, both exhibiting nonzero accessibilities to the quencher. The fluorescence intensity in the absence of quencher F_0 is then given by:

$$F_0 = F_{0a} + F_{0b} \quad (5)$$

where F_{0a} and F_{0b} are fluorescence intensities of the accessible and buried Trps. After application of the Stern-Volmer equation, the fluorescence intensity F at an arbitrary concentration of the quencher $[Q]$ is described by the formula:

$$F = \frac{F_{0a}}{1 + K_a[Q]} + \frac{F_{0b}}{1 + K_b[Q]}. \quad (6)$$

Terms $K_a = \tau_a\, k_{qa}$ and $K_b = \tau_b\, k_{qb}$ stand for the respective Stern-Volmer quenching constants. Substitution for F_{0b} from Eq. (5) to Eq. (6) yields:

$$F = \frac{F_0}{(1 + K_b[Q])} + F_{0a}\left(\frac{1}{1 + K_a[Q]} - \frac{1}{1 + K_b[Q]}\right). \quad (7)$$

The final form of the Stern-Volmer equation for the system with two differently accessible classes of Trps is:

$$\frac{F_0}{F} = \left[\frac{1}{(1 + K_b[Q])} + f_a\left(\frac{1}{1 + K_a[Q]} - \frac{1}{1 + K_b[Q]}\right)\right]^{-1} \quad (8)$$

where f_a is an intensity fraction of the more accessible tryptophans:

$$f_a = \frac{F_{0a}}{F_{0a} + F_{0b}}. \quad (9)$$

Equation (8) converts to the modified Stern-Volmer formula[15] for $K_b = 0$, i.e., for a protein with two classes of Trps one of them being completely inaccessible to the quencher.

Preparation of Samples for FTIR Measurements

Concentrated solutions of TMBP were prepared in 25 mM HEPES/NaO^{2}H p^{2}H 7.5 (buffer A), or in 25 mM HEPES/NaO^{2}H, 10 mM Tre p^{2}H 7.5 (buffer B), or in 25 mM HEPES/NaO^{2}H 10 mM Mal p^{2}H 7.5 (buffer C). The p^{2}H corresponds to the pH meter reading of +0.4.[16] Approximately 1.2 mg of TMBP dissolved in the purification buffer was concentrated to a volume of approximately 40 μL using a "30K Centricon" micro concentrator (Amicon) at 3,000*g* and 4°C. Then 250 μL of buffer A, B, or C was added and the solution was concentrated again. To completely replace the original buffer with the buffer A, B, or C, this procedure was repeated several times. The washings procedure took about 24 h, which is the time of TMBP contact with ^2H_2O before the FTIR analysis. In the last wash, the protein was concentrated to a final volume of approximately 35 μL and used for the FTIR analysis.

FTIR Measurements

The concentrated TMBP samples were placed in a thermostated Graseby-Specac 20500 cell (Graseby-Specac Ltd., Orpington, Kent, UK) fitted with CaF_2 windows and a 25-μm Teflon spacer. FTIR spectra were recorded on a PerkinElmer 1760-x FTIR spectrometer using a deuterated triglycine sulfate detector and a normal Beer-Norton apodization function. At least 24 h before, and during the experiment, the spectrometer was continuously purged with dry air at a dew point of −40°C. Spectra of samples and buffers were acquired at 2-cm^{-1} resolution under the same conditions. In the thermal denaturation experiments, the temperature was increased in 5°C steps from 20° to 95°C using an external bath circulator (Haake F3). Then the step size was decreased and the samples were analyzed at 98°, 99°, and 99.5°C. Temperature in the cell was measured by a thermocouple placed directly onto the CaF_2 windows. The samples were maintained at the desired temperature for 6 min, which is the time necessary for temperature stabilization before the measurement. Spectra were collected and processed using the Spectrum software from PerkinElmer. Subtraction of ^2H_2O was adjusted to the removal of the ^2H_2O bending absorption close to 1,220 cm^{-1}.[17] The deconvoluted parameters were set with a γ value of 2.5 and a smoothing length of 55. Second derivative spectra were calculated over a 5- or 9-data-point range (5 or 9 cm^{-1}).

Generalized 2D-IR Correlation Analysis

The generalized 2D-IR correlation analysis of IR band intensities of deconvoluted spectra was done according to Noda.[18] The method is described in detail elsewhere.[18–20] The 2Dcos toolbox software developed in Prof. Ozaki's Laboratory (Kwansei Gakuin University, Japan) and the Matlab 6.0 (The MathWorks, Inc., Natick, MA) were used for generation of synchronous and asynchronous plots.

MD Simulations

The program Insight II (Version 2000.1, 2000; Accelrys) was used throughout the calculations. The X-ray coordinates of TMBP/Tre at 100 K are available from the Protein Data Bank (PDB)[21] (file 1EU8) and we used them as a starting point for the MD simulations.

Potentials and charges were set before simulations according to CVFF force field, and hydrogen atoms were added with Insight II tools; then, to optimize their geometry, the system was submitted to a mild minimization step using the Steepest Descent method, until a final gradient of 0.5 Kcal · mol^{-1} · Å^{-1} was reached. Then the file was considered suitable for simulation of the starting TMBP/Tre structure. Instead, to simulate unliganded TMBP, the sugar was deleted from the file and the protein was submitted to another minimization step using the Conjugate Gradient method until a final gradient of 0.01 Kcal · mol^{-1} · Å^{-1} was reached. To simulate the TMBP/Mal complex, the coordinates of Mal molecule were extracted from the structure of the complex of Mal with the Mal-binding protein from *E. coli* (PDB file: 1ANF). The molecule was then inserted into the sugar binding cavity of

TMBP with the aid of Insight II tools. To optimize its position, the tool Affinity was used which allows automatic docking of a flexible ligand in a flexible cavity. A grid with 0.5 Å spacing that surrounded movable atoms was created. This created restrains and the parameter files to move the atoms. The resulting complexes were ranked using both the energy check with the Metropolis criterion and the RMS check against structures found in previous cycles. The best ranked complex in a total of five conformations found was chosen as the starting point to simulate the TMBP/Mal structure. The file was submitted to a mild minimization step using the Steepest Descent method, until a final gradient of 0.5 Kcal $\cdot$ mol^{-1} $\cdot$ Å^{-1} was reached. After these modifications, this file was considered suitable to simulate the starting structure of TMBP/Mal.

MD simulations were then applied in all cases with the NVT (constant volume and temperature) ensemble. The temperature was set to 100°C for the full run of 0.2 ns and snapshots of the system were taken every 1 ps. To analyze temperature effects on the geometry of TMBP, TMBP/Mal and the TMBP/Tre complexes, molecules representing "mean" conformations of all structures during the 0.2-ns run were created by "averaging" all conformations obtained, with the aid of the Insight II facilities.

Relative positions and percentages of secondary structure elements were determined using the DSSP program.[22] Solvent accessibility of amino acid residues was evaluated using the program NACCESS[23] by rolling a probe atom of 1.40 Å in radius on the van der Waals surface of the protein models. Identification of H-bonds between TMBP and each of the bound sugars before and after the simulations was done with the program HBPLUS.[24]

RESULTS

Steady-State Fluorescence Spectroscopy

Temperature dependence of fluorescence spectra of TMBP in the absence and in the presence of Mal and Tre is presented in Figure 1. For comparison purposes, all spectra are normalized to the intensity of the unliganded TMBP at 25°C. At all temperatures, TMBP exhibits a broad emission with a spectral shape essentially independent of the presence of ligand. Emission intensity, however, depends on the ligation state of the protein. In particular, the protein fluorescence intensity in the presence of Mal increases about 12%, whereas it decreases about 11% in the presence of Tre. The variations of the protein Trp quantum yield are probably caused by the combined effect of direct interactions of Trp 257 and Trp 295 with the substrate binding[7] as well as by the overall change of the protein structure.

Emission peak of the unliganded TMBP and TMBP/Mal complex is centered near 342 nm. Fluorescence spectrum of TMBP/Tre is slightly blue-shifted with the emission maximum centered near 339 nm. Consistent with the lower Trp quantum yield, this suggests different conformation of TMBP/Tre compared with the TMBP/Mal complex. In the temperature range of 25°–90°C, the spectral positions of all the protein spectra are essentially temperature independent, which it is in agreement with the high thermostability of the protein. All TMBP spectra are blue-shifted compared with the emission of the fully hydrated indole in N-acetyltryptophanamide (NATA) near

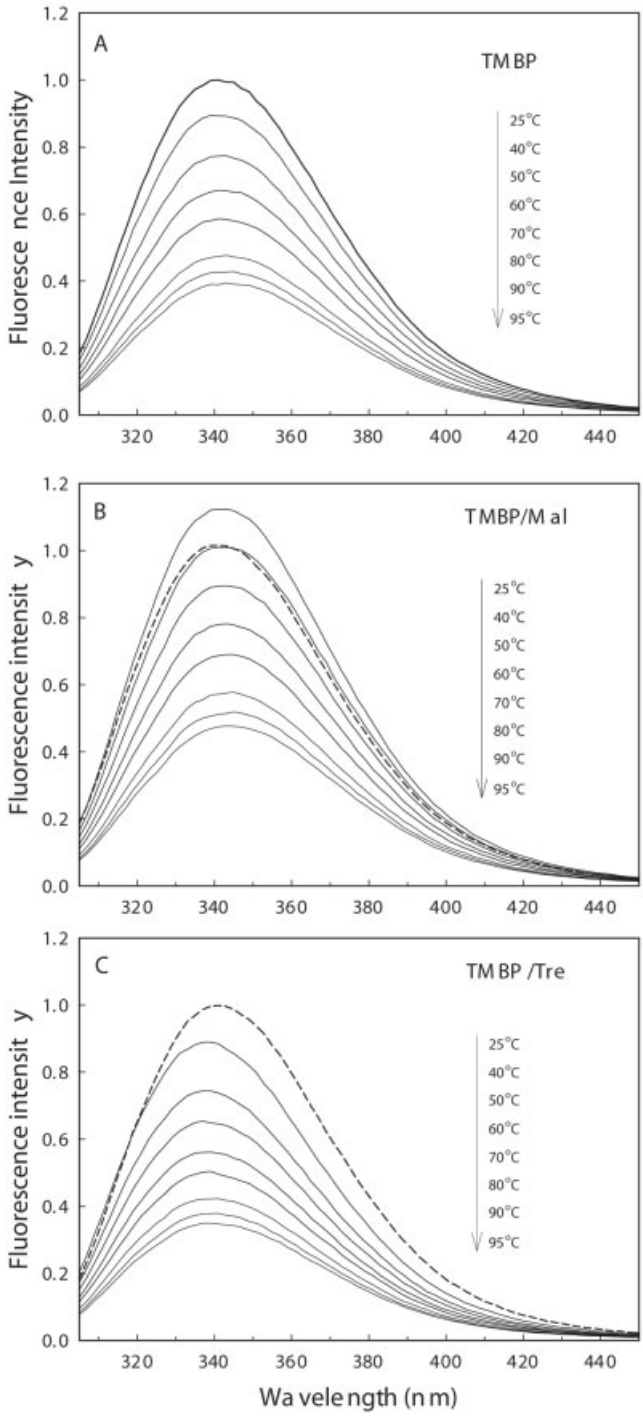

Fig. 1. Fluorescence spectra of TMBP in the absence (**A**) and in the presence of 10 mM Mal (**B**) and Tre (**C**) in the temperature range of 25°–95°C. Spectra are normalized to the intensity of unliganded TMBP at 25°C. Spectrum of TMBP at 25°C is plotted by a heavy dashed line for comparison.

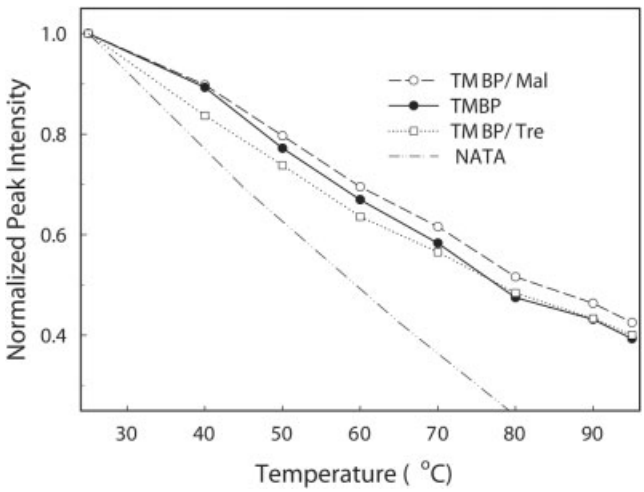

Fig. 2. Temperature dependence of the normalized fluorescence intensity of unliganded TMBP (●), the TMBP/Mal (○), and the TMBP/Tre (□) complex. The intensities were measured at the emission maximum. Temperature quenching of NATA is shown for comparison.[26] Symbols represent experimental data. Lines are the least-square fits.

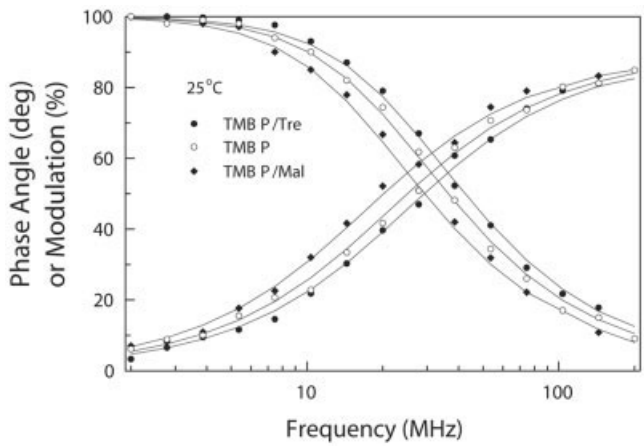

Fig. 3. Phase and modulation frequency responses of TMBP (○), TMBP/Mal (♦), and TMBP/Tre (●) at 25°C. Symbols represent experimental data. Lines are the least-square fits.

352 nm.[25,26] This is an indication that Trps are shielded from the solvent at all temperatures used.

Normalized temperature dependencies of the peak fluorescence intensity are depicted in Figure 2. The melting curves of the TMBP/Mal and TMBP/Tre are dispersed without significant signs of phase transition at temperatures between 25° and 90°C. Unliganded TMBP exhibits a slightly higher slope of the temperature transition with respect to the liganded forms of the protein. However, the protein emission intensity decreases with increasing temperature to a smaller extent than NATA, supporting our suggestion of a protected tryptophan environment in the temperature range of 25°–90°C.

Time-Resolved Fluorescence Spectroscopy

Frequency domain emission decays of TMBP in the absence and in the presence of the two ligands are presented in Figure 3 and in Table I. Visual inspection of the modulation and phase frequency responses reveals that the fluorescence lifetimes depend on the type of the sugar bound. This is indicated by a frequency where the phase and modulation curves intersect. A lower frequency of the intersection indicates a longer fluorescence lifetime. It can be seen that the mean lifetime increases as follows: $\bar{\tau}$ (TMBP/Tre) $< \bar{\tau}$ (TMBP) $< \bar{\tau}$ (TMBP/Mal). This observation is consistent with the steady-state data. Because the frequency domain emission decays did not support more complicated decay models, we fitted them by the two exponentials model. At room temperature, the decays were found to be nearly monoexponential. At higher temperatures, a short-component lifetime τ_1 showed up causing an increase of the decay heterogeneity. The intensity fraction of the short component increased from a few percent at 60°C up to around 15% at 90°C (Table I). It has to be stressed that, for TMBP with 12 Trp residues, a unique assignment of the lifetime components is problematic. The mean fluorescence lifetime $\bar{\tau}$ is therefore a preferable quantity reflecting collective emission properties and interactions of all Trp residues.

Temperature dependence of $\bar{\tau}$ is also presented in Table I. It is seen that at all temperatures the presence of Mal and Tre causes increase and shortening of $\bar{\tau}$, respectively. This behavior is consistent with the steady-state data (Fig. 1) that show the protein fluorescence quenching upon the Tre binding. An opposite protein fluorescence behavior was recorded upon Mal binding. This is an additional indication that TMBP can exist in three different conformational states: TMBP alone, TMBP/Mal, and TMBP/Tre.

Fluorescence Quenching Experiments

To further explore influence of the sugars on the TMBP conformation, we examined temperature-induced changes of TMBP packing by evaluating Trp accessibility to the fluorescence quencher, acrylamide. Quenching experiments were done both in the presence and in the absence of Mal and Tre. Figure 4(A–C) shows the steady-state fluorescence quenching at 25°, 60°, and 90°C, respectively. It is seen that the Stern-Volmer (SV) plots of the protein/sugar complexes are roughly linear at all temperatures [Fig. 4(A–C), open symbols]. Linearity of the plots indicates absence of a large Trp fraction with significantly different accessibilities to the quencher. Table II presents the calculated SV and bimolecular quenching constants of the systems. K_{sv} of the TMBP/Mal complex is essentially temperature independent with the value being close to 0.18 M^{-1}. The K_{sv} of the TMBP/Tre complex is 0.28 M^{-1} at 25°C and slightly decreases with temperature. All K_{sv} are significantly lower than 15.9 M^{-1} which is a K_{sv} of free Trp in water.[23] At room temperature, the bimolecular quenching constants k_q of the complexes are more then 85 times lower than the value of 5.9×10^9 $M^{-1}s^{-1}$ reported for free Trp.[23] Measured k_q values report about high inaccessibility of Trp residues to acrylamide as a consequence of dense protein packing. The packing of TMBP/Mal seems to be especially dense because the complex exhibits at all tem-

TABLE I. Trp Fluorescent Lifetimes of TMBP in the Absence and in the Presence of a Saturating Amount of Mal and Tre

Temperature (°C)	τ_1 (ns)[a]	τ_2 (ns)	α_1	α_2	f_1	f_2	$\bar{\tau}$ (ns)
TMBP							
25	—	7.57	—	1.00	—	1.00	7.57
60	0.05	6.25	0.90	0.10	0.06	0.94	5.84
90	0.07	5.22	0.93	0.07	0.16	0.84	4.40
TMBP/Mal							
25	—	9.41	—	1.00	—	1.00	9.41
60	0.09	7.92	0.74	0.26	0.03	0.97	7.66
90	0.04	5.87	0.96	0.04	0.13	0.87	5.12
TMBP/Tre							
25	—	6.50	—	1.00	—	1.00	6.50
60	0.02	5.42	0.90	0.10	0.03	0.97	5.24
90	0.03	4.47	0.97	0.03	0.18	0.82	3.69

[a]Standard errors are 0.10 and 0.2 ns for τ_1 and τ_2, respectively.

peratures about twice lower k_q than TMBP/Tre. A different quenching pattern was found for the unliganded TMBP. Figure 4 show that the unliganded TMBP is more susceptible to temperature changes. At room temperature, consistent with the steady-state and the time-resolved data, the value of $K_{sv} = 0.24\ M^{-1}$ lies between the K_{sv} of TMBP/Mal and the one of TMBP/Tre [Fig. 4(A), Table II]. With increasing temperature, the quenching efficiency of TMBP fluorescence gradually increases. At 90°C, the character of the quenching dramatically changes and the SV-plot becomes strongly nonlinear [Fig. 4(C)]. The downcurve of the SV-plot usually indicates presence of Trp residues with significantly different accessibilities to the quencher.[8,15]

To account for this nonlinearity, we fitted the data with the model that accommodates two classes of Trp residues [Eq. (7)]. Because the SV-constants K_a and K_b in Eq. (7) are highly correlated which prevents their reliable simultaneous fitting, we arbitrarily fixed K_b of the buried Trps to $0.3\ M^{-1}$. Then we adjusted K_a only. The fixed value of K_b seems to be a reasonable estimate because it is an extrapolation of the temperature dependence of K_{sv} for TMBP from Table II. Moreover, the value closely agrees with the slope of the SV-plot at high acrylamide concentrations ($0.32\ M^{-1}$), when the accessible Trps are supposed to be already quenched [Fig. 4(C), dashed line]. Under this assumption, the value of K_a is $2.3\ M^{-1}$ and the intensity fraction f_a of the accessible Trps is 44%. From the SV-plots we conclude that the residue packing of some domain in the sugar-free TMBP significantly loosens with increasing temperature and, as a consequence, some of the Trp residues become more accessible to acrylamide. The rest of the protein structure remains compact with packing similar to the one of the TMBP/sugar complexes.

Estimates of the bimolecular quenching constants are given in Table II. It has to be stressed that for the system with 12 Trp residues it is unrealistic to resolve and uniquely assign lifetime components. Therefore, we have to use estimates of fluorescence lifetimes for calculation of k_{qa} and k_{qb}. The k_{qb} was calculated assuming the lifetime of 4.4 ns from Table I. This value was also used for calculating the low estimate of $k_{qa.}$ The high estimate of k_{qa} was based on the Trp lifetime of 0.5 ns at 90°C. This value was also used for calculating the low estimate of k_{qa}. The high estimate of k_{qa} was based on the Trp lifetime of 0.5 ns at 90°C. This value was estimated from the mean Trp lifetime of 2.7 ns at 25 °C[27] corrected for temperature dependence of NATA emission.[26,27] Even though we recognize that the values of k_{qa} and k_{qb} can be to some extent biased by these assumptions, the data strongly indicate opening of the unliganded TMBP structure around 90°C.

FTIR Measurements

To gain more information on temperature-induced structural changes of TMBP in the absence and in the presence of Mal or Tre, we performed FTIR absorption measurements. The FTIR technique is sensitive to secondary structure changes as well as to subtle structural changes influencing, e.g., solvation degree of secondary structure elements or protein packing that modulates the rate of the $^1H/^2H$ exchange. Figure 5 shows absorbance (A), resolution enhanced deconvoluted (B), and second derivative (C) infrared spectra of TMBP at 20°C. Within the 1,700 cm^{-1} −1,620 cm^{-1} interval, encompassing the amide I′ band, the deconvoluted and second derivative spectra show a number of bands assignable to secondary structural elements.[28,29] The presence of β-sheets is revealed by the 1,635.6, 1,690.1, and the 1,676 cm^{-1} bands. The assignment of the latter band is less certain because also turns may contribute to this frequency.[29,30] The 1,625 cm^{-1} shoulder could be caused either by intermolecular interactions, by unusually strongly hydrogen-bonded β-sheet, or by some particularly solvent-exposed β-strands.[29,31] The 1,667 and 1,645 cm^{-1} bands may be ascribed to turns and unordered structures, respectively, whereas the 1,651.1 and 1,658 cm^{-1} bands are vibrations of α-helices. The latter band originates probably from the less solvent-exposed helices.[29,32] Bands less than 1,620 cm^{-1} are caused by absorption of amino acid side-chains. In particular, the 1,515.2 cm^{-1} band originates from vibrations of tyrosines, the 1,565.5 cm^{-1} band is caused by ionized glutamic acids, and the 1,580.7 cm^{-1} band may be as-

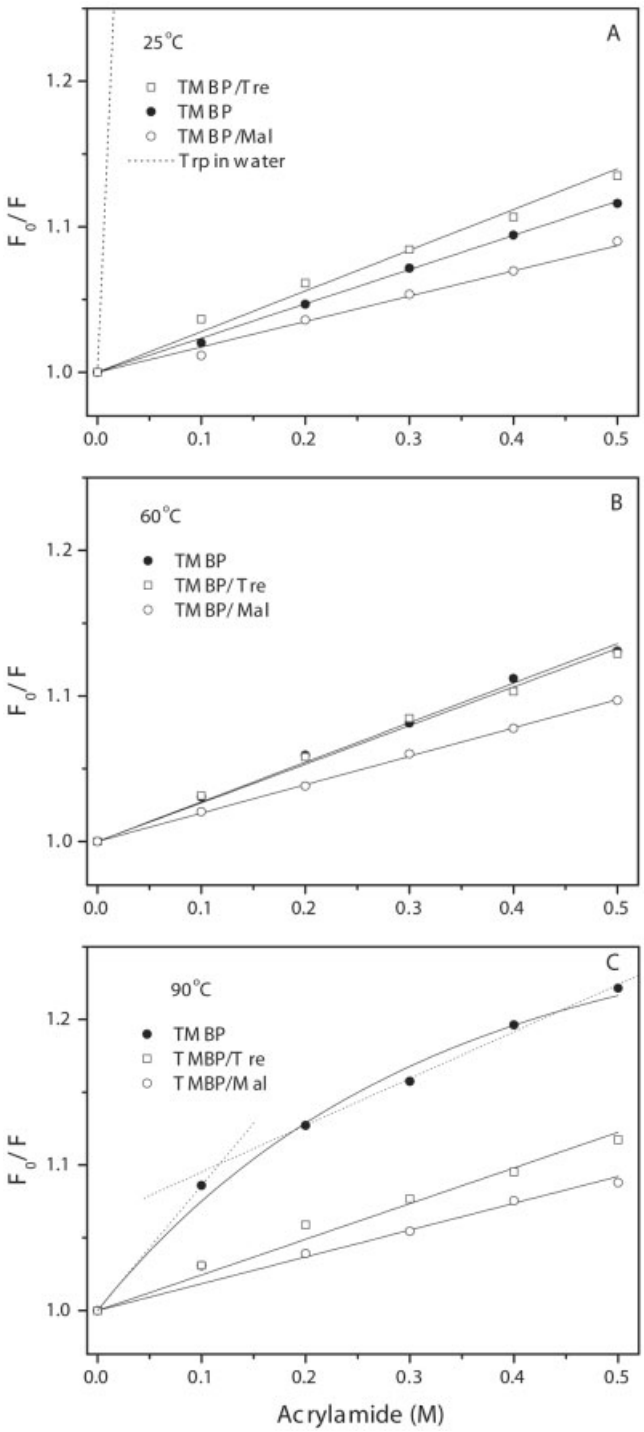

Fig. 4. Steady-state acrylamide quenching of TMBP fluorescence at 25° (**A**), 60° (**B**), and 90°C (**C**) in the absence (●) and in the presence of 10 mM Mal (○) and 10 mM Tre (□). Collisional fluorescence quenching of free Trp in water at 25°C is given for comparison (dotted line), assuming that the Trp lifetime in the aqueous environment is 2.7 ns and the bimolecular quenching constant of Trp by acrylamide, k_q, is 5.9×10^9 $s^{-1}M^{-1}$.[27] Solid lines represent the best data fits.

signed to ionized carboxyl groups of aspartic acid and/or to arginyl residues.[33,34] The 1,548.1 cm^{-1} band represents a residue of the amide II band, i.e., the residual absorption after $^1H/^2H$ exchange of the amide hydrogens of the polypeptide chain. In fact, in the ^1H_2O medium, the intensity of the amide II equals about 2/3 of the amide I intensity (data not shown). In ^2H_2O medium, the intensity of the amide II band decreases as a consequence of the exchange of amide hydrogens with deuterium.[35] The larger the decrease in the amide II intensity, the larger the extent of the $^1H/^2H$ exchange indicating a better accessibility of protein residues to the solvent (^2H_2O). The weak 1,548.1 cm^{-1} band indicates that a small amount of amide hydrogens were not exchanged with deuterium during the preparation of the protein sample.

Figure 6 shows a comparison of resolution-enhanced spectra of unliganded TMBP and the TMBP/Mal and TMBP/Tre complexes at room temperature. Both sugars induce small, but significant changes in the FTIR spectra. In particular, the main β-sheet band shifts slightly to a higher wavenumber suggesting a lower accessibility of the solvent (^2H_2O) to this structural element. This finding is consistent with the crystallographic data indicating that bound Tre forms H-bonds with β-strands of the protein.[7] This small decrease in solvent accessibility is supported by the slightly higher intensity of the residual amide II band in the sugar-bound TMBP compared with the unliganded protein. The crystal structure of TMBP/Tre complex suggests that three Asp residues, two Arg, and two glutamic residues take part in the H-bonding with the sugar in the binding site.[7] This finding may explain small differences in the 1,565.5 and 1,580.7 cm^{-1} band intensities of Glu and Asp (and/or Arg), respectively, that were observed in the spectra of the sugar-bound TMBP compared with the unliganded TMBP spectrum. In addition, the FTIR spectra indicate that the sugar binding does not induce changes in the secondary structure because the intensities of the amide I′ component bands do not change.

Thermal Stability

Increase in temperature causes changes in FTIR spectra of TMBP as shown in Figure 7. Comparison of the spectra collected at 20°C (bottom) and 99.5°C (top) indicates that the temperature induces only partial denaturation of the protein because the α-helix and β-sheet bands dominate the spectra at all temperatures. The melting of the protein is indicated by a decrease in the amplitude of these bands. At the highest temperatures, the spectra reveal a strong band at 1,616 cm^{-1} caused by protein aggregation.[36] This band first appears at 90°C suggesting that, at high protein concentrations needed for the FTIR measurements (~35 mg/mL), the denaturation/aggregation process starts close to this temperature. Difference spectra in Figure 8 confirm this conclusion. The spectra were calculated by subtracting successive spectra collected at stepwise increasing temperature. A negative band indicates a decrease of a particular secondary structure with increased temperature and vice versa. Hence, the broad negative band between 1,600 and 1,700 cm^{-1} indicates a loss of secondary structure at higher temperature whereas the two positive peaks close to 1,616 and 1,685 cm^{-1} represent protein aggregation brought about by thermal denatur-

TABLE II. Stern-Volmer (K_{SV}) and Bimolecular Quenching Constants (k_q) of TMBP Fluorescence Quenched by Acrylamide in the Absence and the Presence of Mal and Tre

Temperature (°C)	TMBP					TMBP/Mal[c]		TMBP/Tre[d]	
	K_{SV} (M^{-1})[a]			k_q ($M^{-1}s^{-1}$)[b]		K_{SV} (M^{-1})[a]	k_q ($M^{-1}s^{-1}$)[b]	K_{SV} (M^{-1})[a]	k_q ($M^{-1}s^{-1}$)[b]
25	0.24			3.2×10^7		0.17	1.8×10^7	0.28	4.4×10^7
60	0.27			4.6×10^7		0.19	2.5×10^7	0.27	5.3×10^7
90	K_a[e]	K_b[e]	f_a[e]	k_{qa}[f]	k_{qb}[g]	0.18	3.5×10^7	0.25	6.9×10^7
	2.3	0.3[h]	0.44	$(52-460) \times 10^7$	6.8×10^7				

[a]Stern-Volmer quenching constant from Eq. (4).
[b]Bimolecular quenching constant from Eq. (4).
[c]5 mM Mal.
[d]5 mM Tre.
[e]Parameters from Eq. (8).
[f]The low estimate of the bimolecular quenching constant was calculated using $\tau = 4.4$ ns from Table I. The high estimate was based on the Trp lifetime of 0.5 ns at 90°C. This lifetime was estimated by using Trp lifetime of 2.7 ns at 25°C[27] and a temperature quenching of NATA fluorescence.[26]
[g]Bimolecular quenching constant calculated using $\tau = 4.4$ ns from Table I.
[h]Value estimated from the slope of the Stern-Volmer plot at high acrylamide concentrations.

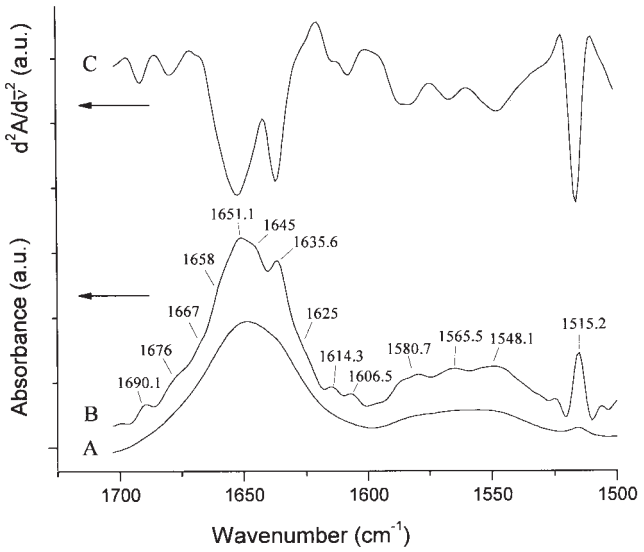

Fig. 5. Absorbance (**A**), deconvoluted (**B**), and second derivative (**C**) IR spectra of TMBP at 20°C. The protein was diluted in 25 mM HEPES/NaO^{2}H buffer, p^{2}H 7.5. The deconvoluted parameters were set with a γ value of 2.5 and a smoothing length of 55. The second derivative spectrum was calculated over a nine-data-point range (9 cm^{-1}). The second derivative spectrum calculated over five-data-point range displayed the same amide I′ component bands as those reported in the deconvoluted spectrum (data not shown).

ation.[36,37] The negative 1,546 cm^{-1} band mainly represents an enhanced $^1H/^2H$ exchange caused by increased temperature and by the protein unfolding.[37] Inspection of the difference spectra in Figure 8 reveals that the loss of the secondary structure starts close to 90°C. This temperature correlates with the protein aggregation starting around 85°–90°C in all cases. We found that at 99.5°C, both the loss of the secondary structure and the protein aggregation are remarkably slow because the spectra of protein maintained at 99.5°C for 30 min did not dramatically change the shape [spectrum (h)]. This indicates particular thermostability of the remaining structural elements that is not significantly affected by the sugar binding.

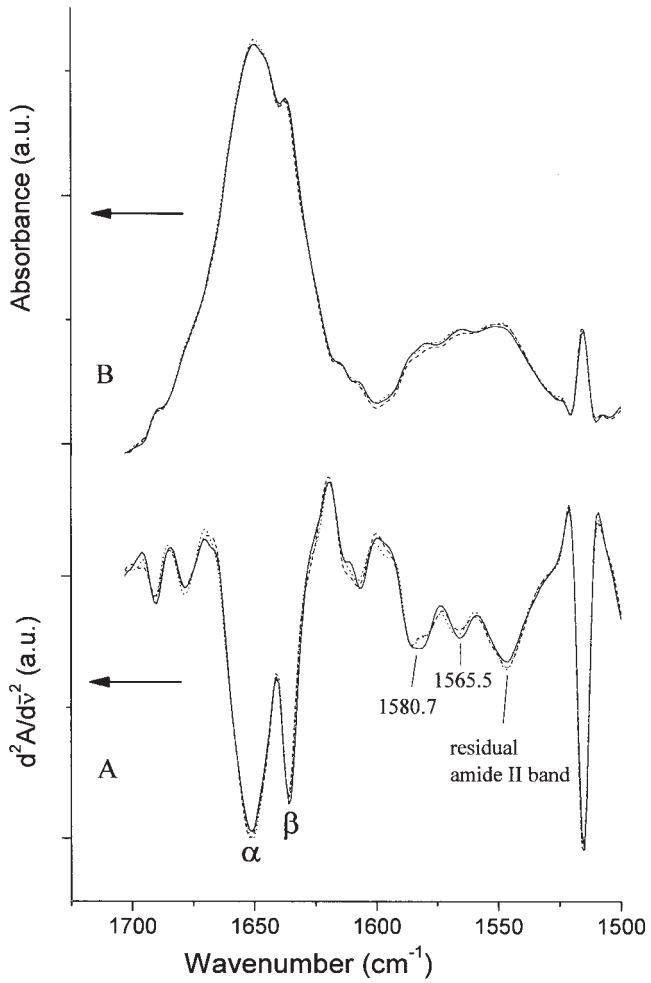

Fig. 6. Second derivative (**A**) and deconvoluted (**B**) spectra of TMBP in the absence and in the presence of Mal or Tre at 20°C. Continuous line refers to TMBP, dotted and dashed lines refer to TMBP/Mal and TMBP/Tre, respectively. The deconvoluted parameters were set with a γ value of 2.5 and a smoothing length of 55. Second derivative spectrum was calculated over a nine-data-point range (9 cm^{-1}).

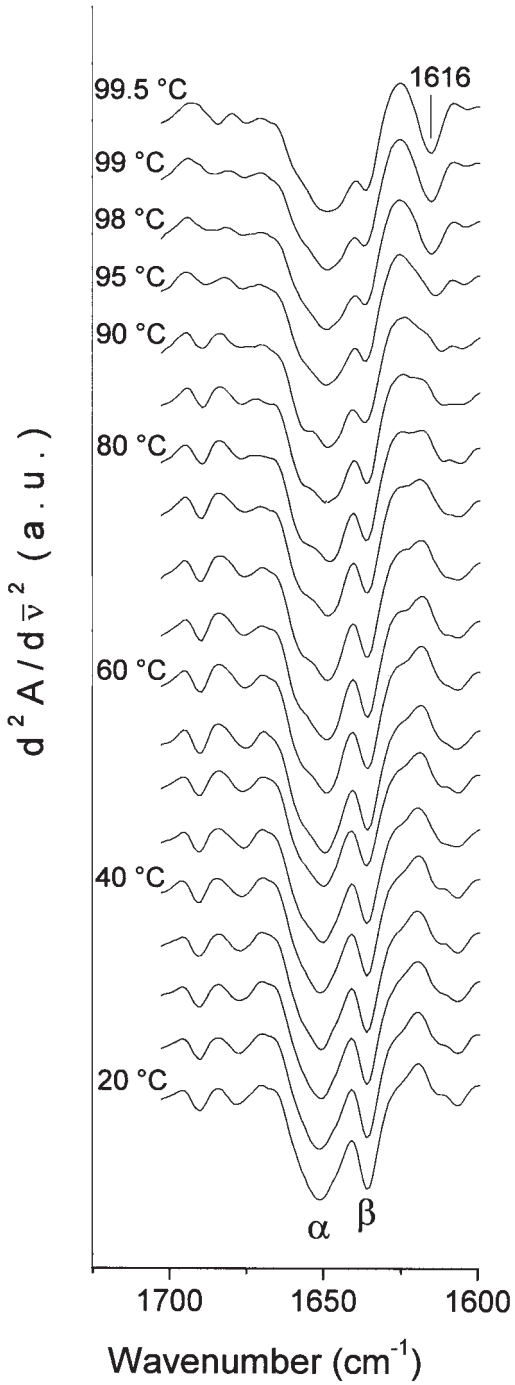

Fig. 7. Temperature-dependent changes in the second derivative spectra of TMBP. Second derivative spectra were calculated over a nine-data-point range (9 cm^{-1}). Spectra are reported in 5°C steps from 20°C (**bottom**) to 95°C. The last three spectra (**top**) are recorded at 98.0°C, 99.0°C, and 99.5°C. The band at 1,616 cm^{-1} indicates protein aggregation.

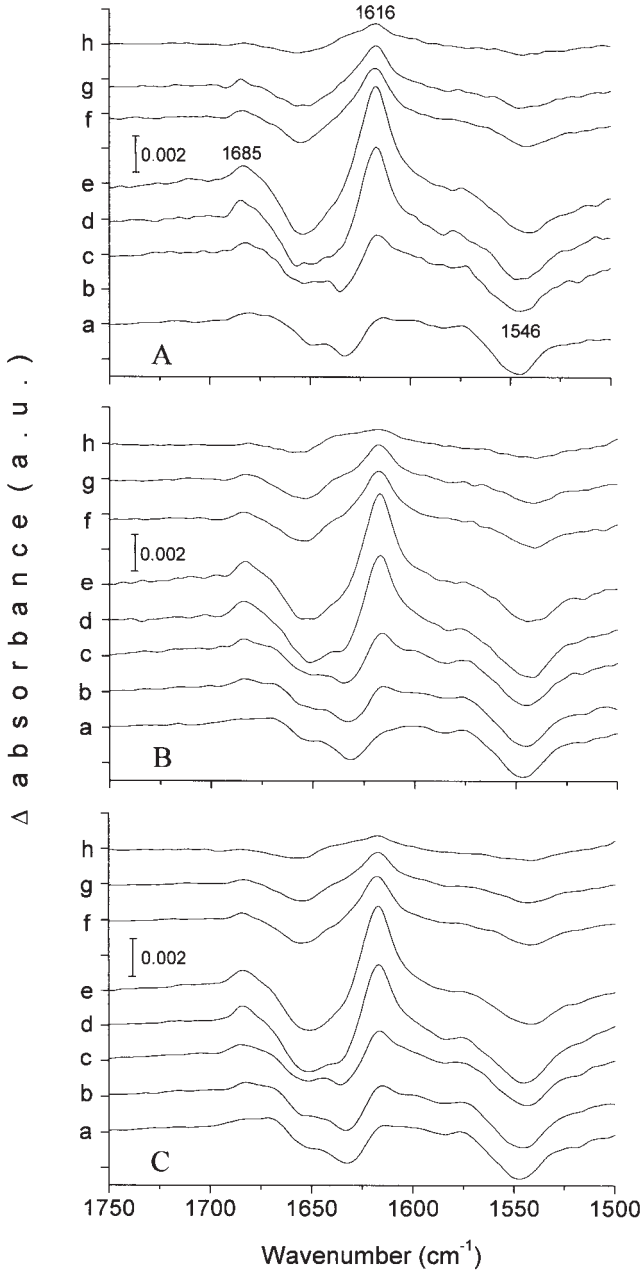

Fig. 8. Differential spectra of TMBP (**A**), TMBP/Mal (**B**), and TMBP/Tre (**C**) calculated as difference between two original absorbance spectra collected at different temperatures. Spectra (**a–g**) represent the difference between the absorbance spectra collected at: 80°C–75°C, 85°C–80°C, 90°C–85°C, 95°C–90°C, 98°C–95°C, 99°C–98°C, and 99.5°C–99.0°C. The differential spectrum (**h**) refers to the difference between two absorbance spectra collected at 99.5°C at two different times (30 min and 0 min).

We now provide further details on temperature-induced structural changes obtained from the second derivative spectra collected at 85°C (Fig. 9). This is an optimum growth temperature of *T. litoralis*.[12] Figure 9 shows that the 1,658 cm^{-1} band belonging to poorly solvent-exposed α-helices is weaker in the spectra of TMBP/Mal and TMBP/Tre. On the contrary, the 1,651 cm^{-1} band of solvent-exposed α-helices has higher amplitude in the spectra of the complexes than in the spectrum of the unliganded TMBP. This suggests that at the optimal-growth temperature the sugar binding induces conformational change causing the buried α-helices to become more solvent exposed.

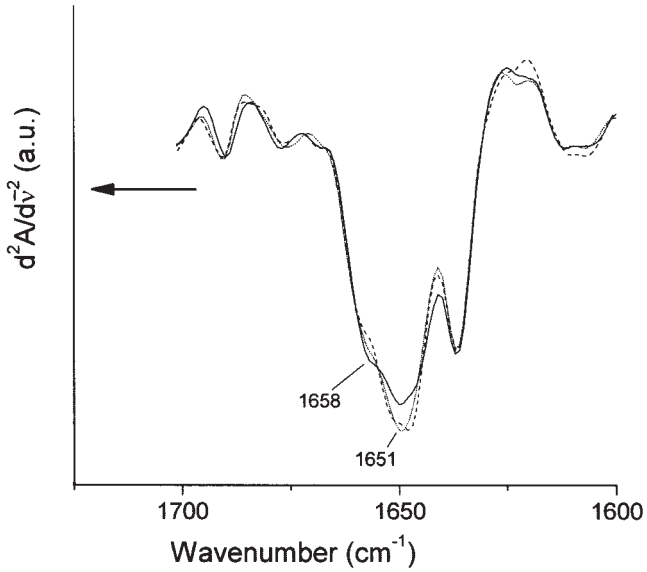

Fig. 9. Second derivative spectra of TMBP, TMBP/Mal, and TMBP/Tre at 85°C. Continuous line refers to TMBP, dashed and dotted lines refer to TMBP/Mal, and TMBP/Tre, respectively. The spectra were calculated over a nine-data-point range (9 cm^{-1}).

TABLE III. Sequence of Temperature-Induced Events for TMBP Monitored Using IR Experiments

Temperature	Wavenumber (cm^{-1})[a]
20°C	1,516 ↓[b], 1,550 ↓, 1,634 ↓
↓	1,651 ↓,
99.5°C	1,659 ↓,
	1,617 ↑, 1,685 ↑

[a]1,516 cm^{-1} (tyrosine); 1,550 cm^{-1} ($^1H/^2H$ exchange); 1,634 cm^{-1} (β-sheets); 1,651 cm^{-1} (α-helices); 1,659 cm^{-1} (α-helices); 1,617 cm^{-1} (protein aggregation); 1,685 cm^{-1} (protein aggregation).
[b]Symbols (↑) and (↓) mean the increase and the decrease of the peak intensity, respectively.

Thermal Unfolding Monitored by Generalized 2D Correlation Analysis of IR Spectra

To obtain more details on the thermal stability and thermal unfolding of the protein, we applied generalized 2D-IR correlation analysis on the infrared spectra collected at different temperatures. The method generates synchronous and asynchronous spectra of the dynamic spectral intensity variation induced by an external perturbation. A combination of the plots provides details on the sequence of events following the perturbation.[18–20] The 2D-IR spectra of TMBP/Mal and of TMBP/Tre were identical to those of TMBP (spectra not shown) indicating that the sugar binding does not affect the sequence of the thermal unfolding events. The data reported in Table III indicate that the early events occurring with the increase in temperature are the concomitant decrease in intensity of the Tyr band (1,516 cm^{-1}), of the residual amide II band (1,550 cm^{-1}), and of the β-sheet band (1,634 cm^{-1}). Then, a decrease in intensity of the 1,651 cm^{-1} band (exposed α-helices) followed by the decrease in intensity of the 1,659 cm^{-1} band (buried α-helices) occurs. The 2D-IR data indicate that β-sheets start unfolding before α-helices and that the solvent-exposed helices are more temperature-sensitive than the buried ones. The ultimate temperature-dependent event is the protein aggregation brought about by the thermal denaturation and indicated by the appearance of the 1,617 and 1,685 cm^{-1} aggregation bands.

TABLE IV. Summary of MD Simulation Results

Secondary structures (%)	TMBP	TMBP/Tre	TMBP/Mal
α-Helices[a]	42.3	39.1	41.0
β-Structures[b]	13.5	12.5	14.7
Others[c]	24.5	27.0	25.1
Random coil[d]	19.7	21.4	19.2
Solvent accessibility (%)[e]			
Trp 21	1.0	0	0
Trp 73	0.5	1.5	0.1
Trp 82	7.2	18.3	4.4
Trp 146	3.8	5.3	1.9
Trp 168	14.1	13.8	12.0
Trp 172	1.4	0.2	0.1
Trp 203	2.7	4.3	1.8
Trp 257	16.5	0	0.3
Trp 261	13.4	10.6	8.1
Trp 295	10.0	1.8	0.5
Trp 310	1.8	1.0	0.5
Trp 331	2.6	1.2	0.3
Mean accessibility (%)[f]	6.2	4.8	2.5

[a]Marked as "H" in DSSP output.
[b]Marked as "E" in DSSP output.
[c]Marked as "B," "G," "I," "T," "S" in DSSP output.
[d]Not classified in DSSP output.
[e]All Trp atoms.
[f]The mean of all Trp accessibilities.

MD Simulations

To gain insight into the experimentally accessed differences in structural TMBP properties caused by sugar binding at high temperatures, we performed MD simulations on unliganded TMBP and TMBP/Tre, TMBP/Mal complexes. Figure 10 shows a comparison of the average structures of TMBP (panel A), TMBP/Tre (panel B), and TMBP/Mal (panel C) after 0.2 ns of MD simulations at 100°C. Visual inspection suggests that these 3D structures are similar to each other and do not differ much from the starting X-ray structure (panel D). In all systems, the secondary structures are largely intact after exposure to high temperatures. Table IV (top) shows a comparison of the secondary structure percentages calculated with the DSSP program on the simulated structures of TMBP, TMBP/Tre, and TMBP/Mal. This analysis confirms that there are only insignificant differences in percentages of the secondary structure elements between all calculated structures. This supports conclusions from the IR spectroscopy. Table IV (bottom) shows calculated Trp accessibilities to the solvent which can be compared with measured quenching efficiencies. We can identify that main differences in Trp accessibilities between the TMBP, TMBP/Mal, and the TMBP/Tre structures are located on Trp 257, Trp 295, Trp 82, and Trp 261. The first two Trp residues

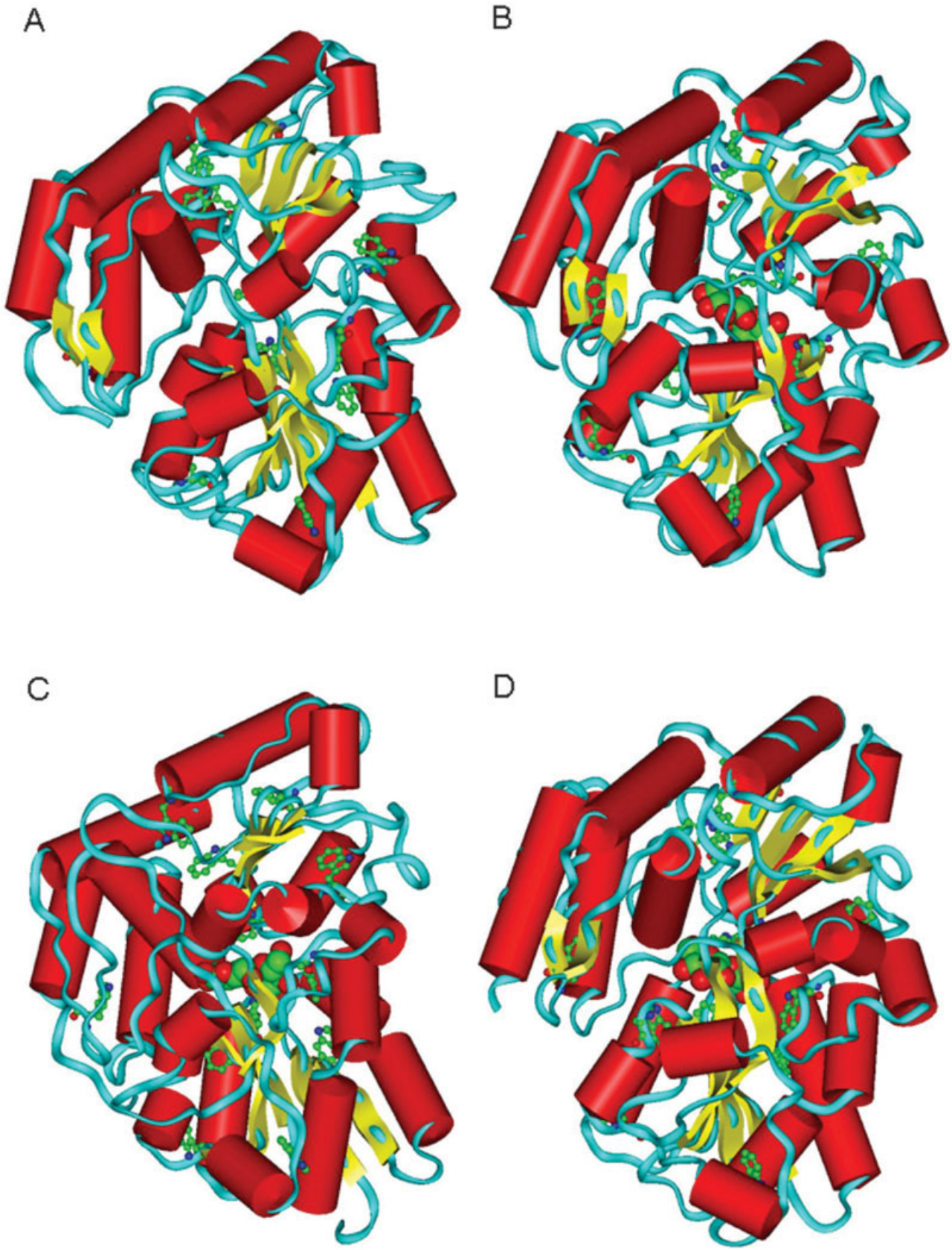

Fig. 10. Results of MD simulation. Average structures of TMBP (**A**), TMBP/Tre (**B**), and TMBP/Mal (**C**) after the 0.2ns MD run at 100°C. As a comparison, the X-ray structure of TMBP/Tre is showed in panel (**D**). Helices and sheets are shown as red cylinders and yellow ribbons, respectively. Tryptophan residues are shown in ball and stick mode. In panels B, C, and D, the sugars bound to TMBP are shown in the CPK mode. Atom type color codes: carbon green, oxygen red, nitrogen blue.

are involved in the sugar binding[7] and it should not be surprising that in the absence of the sugar their accessibility to solvent significantly increases. This can also explain quenching data at 90°C indicating the presence of accessible and inaccessible classes of Trp in the protein at this temperature. It is of interest why fluorescence quenching does not exhibit signs of such high Trp accessibility at low and intermediate temperatures. A possible explanation could be that at low temperatures this hyperthermophilic TMBP assumes a rigid conformation with restricted accessibility to the sugar binding site. Alternatively, configuration of the binding site could be "distorted" at low temperature with Trp 257 and Trp 295, normally participating in the sugar binding, buried. A proof of such hypothesis, however, needs more experimental evidence even though it is indirectly supported by the fact that successful crystallization of TMBP required the protein to be incubated with saturation amount of Tre at 80°C.[7] Calculations indicate that solvent accessibility of Trp 82 increases upon Tre binding whereas the opposite is true for Trp 82 of TMBP/Mal complex. Trp 261 becomes progressively more shielded from TMBP to TMBP/Tre to TMBP/Mal. Finally, simulated mean Trp accessibilities to the solvent are given in the last line of Table IV. Simulations show that unliganded TMBP exhibits significantly higher mean Trp accessibility than the sugar-bound forms, TMBP/Mal being less accessible than the TMBP/Tre complex. This observation fully agrees with the acrylamide quenching at 90°C. We also analyzed interactions of the sugars with TMBP, by means of the HBPLUS program. In the starting structures of TMBP/Tre and TMBP/Mal, the moieties of the first glucose Glc1, as identified in ref.[7] are almost superimposed, and the second glucose ring shows a slightly different orientation, with the C6′ atom of Mal pointing in the same direction as O2′ of Tre. It is worth stating that the binding mode of the two disaccharides is different, because Tre forms six H-bonds with four different residues, whereas Mal forms five H-bonds with three different residues (data not shown). After the MD runs, we notice for both complexes a decrease of the number of H-bonds. The sugar, however, is still present in the binding cavity and it does not lose contact with the protein.

DISCUSSION

Because several conclusions were derived from the fluorescence quenching, it is useful to examine whether the observed changes of k_q are not a simple consequence of changed water viscosity at different temperatures. In the first approximation, the diffusion coefficient D of the quencher is described by the Stokes-Einstein equation, $D = kT/6\pi\eta R$. Therefore, the k_q should be proportional to the ratio of T/η, where T is temperature in Kelvin and η is the viscosity of water at the temperature T. If the change of the k_q was a consequence of the changed temperature and the water viscosity only, the ratio $G = (k_q)_{T1}/(k_q)_{T2}$ should be equal to $(T_1 \cdot \eta_2)/T_2 \cdot \eta_1$, where $(k_q)_{T1}$ and $(k_q)_{T2}$ are the bimolecular quenching constants at temperatures T_1 and T_2, respectively. For water at $T_1 = 60$°C and $T_2 = 25$°C, the ratio $(k_q)_{60C}/(k_q)_{25C}$ should be equal to $(333K/\eta_{60C})/(298K/\eta_{25C})$ which is close to 2.1.[38] The experimentally measured ratio $(k_q)_{60C}/(k_q)_{25C}$ has a significantly lower value ranging from 1.2 for TMBP/Tre complex to 1.39 for the TMBP/Mal and 1.44 for unliganded TMBP. Similar behavior was observed for liganded TMBP at highest temperatures when the measured ratio $(k_q)_{90C}/(k_q)_{60C}$ was 1.3 and 1.4 for TMBP/Tre and TMBP/Mal, respectively, and the predicted ratio was close to 1.6. The smaller k_q increase than the predicted one is a consequence of Trp shielding and a sign of dense residue packing. Similar behavior has previously been found for the glucose-galactose binding protein in the presence of glucose.[39] Quenching data indicate that at 90°C the TMBP structure partially opens, which results in a dramatic increase of the bimolecular quenching constant. The high estimate of k_{qa} from Table II, however, is still more than four times smaller than the value of 20×10^9 $M^{-1}s^{-1}$ estimated from published k_q[27] and temperature dependence of water viscosity[38] for free Trp at his temperature.

The optimum growth temperature (t-optimum) of *T. litoralis* is about 85°C. At this temperature, the archaeal TMBP-dependent ABC transporter exhibits peak activity (K_m = 20 nM) and high affinity to Tre (K_d = 0.16 μM), whereas at room temperature the activity is less then 5%.[4,12] Our data show that, while at room temperature both unliganded and sugar-bound structures are highly rigid, around t-optimum the unliganded TMBP opens and dense packing of the protein partially relaxes. This is in marked contrast with behavior of the TMBP/Mal and TMBP/Tre complexes that remain densely packed even at high temperatures. Because binding of substrate is brought about by a movement of two protein lobes as reported for similar protein from *E. coli*,[9] the temperature-induced TMBP relaxation seems to be important for efficient protein function. Difficulties with crystallizing any ABC transporter complexes from mesophilic organisms[40] are aligned with our observation of loosened TMBP packing and consequent high segmental mobility at t-optimum.

In conclusion, we have documented by FTIR, fluorescence, and MD methods that TMBP exhibits remarkable temperature stability. Although the secondary structure is not significantly affected by sugar binding, the protein assumes different conformations depending on the particular sugar bound to the protein. The TMBP/Mal complex was found to be more compact with respect to the TMBP/Tre one and unliganded TMBP exhibits signs of relaxed packing at the optimal growth temperature. A general assumption is that ligand binding should stabilize the protein and reduce protein dynamics.[41,42] However, numerous reported studies proved that ligand binding enhanced segmental motion of the protein.[43–46] So far, the effect of the ligand binding on the protein structure cannot be predicted with certainty and it has to always be experimentally evaluated.

The new insight to the dynamics and stability of TMBP contributes not only to better understanding of transport-related functions of binding protein-dependent ABC transporters, but it also constitutes ground for development of biotechnological applications requiring thorough structure-

functional characterization of the system before a targeted mutation and/or labeling is performed. This task could be a development of an extremely thermostable biosensor for monitoring of glucose level in blood. The recombinant TMBP seems to be a good candidate for this task. This work is in progress.

ACKNOWLEDGMENTS

The authors thank Dr. Fabienne Chevance, University of Utah, Salt Lake City, UT, for supplying a partially purified protein sample, and Dr. Susan Costantini, Laboratory of Bioinformatics, ISA, Avellino, for providing a tool for the calculation of the percentage of secondary structures from a DSSP file. This work was supported by a NATO-CNR grant to P.H., a grant from the Ministry of Education, Youth and Sports of the Czech Republic to P.H., FIRB grant to M.R. and S.D., a grant from Università Politecnica delle Marche (Ricerca di Ateneo) (F.T.), and CRdC-ATIBB POR UE-Campania Mis. 3.16 activities (S.D., M.R.), and by the CNR Commessa Diagnostica avanzata ed alimentazione (S.D.).

REFERENCES

1. Gilson E, Alloing G, Schmidt T, Claverys JP, Dudler R, Hofnung M. Evidence for high affinity binding-protein dependent transport systems in gram-positive bacteria and in mycoplasma. EMBO J 1988;7(12):3971–3974.
2. Herrmann A, Schlosser A, Schmid R, Schneider E. Biochemical identification of a lipoprotein with maltose-binding activity in the thermoacidophilic Gram-positive bacterium *Alicyclobacillus acidocaldarius*. Res Microbiol 1996;147(9):733–737.
3. Sahm K, Matuschek M, Muller H, Mitchell WJ, Bahl H. Molecular analysis of the amy gene locus of *Thermoanaerobacterium thermosulfurigenes* EM1 encoding starch-degrading enzymes and a binding protein-dependent maltose transport system. J Bacteriol 1996;178(4):1039–1046.
4. Xavier KB, Martins LO, Peist R, Kossmann M, Boos W, Santos H. High-affinity maltose/trehalose transport system in the hyperthermophilic archaeon *Thermococcus litoralis*. J Bacteriol 1996;178(16): 4773–4777.
5. Albers SV, Elferink MG, Charlebois RL, Sensen CW, Driessen AJ, Konings WN. Glucose transport in the extremely thermoacidophilic *Sulfolobus solfataricus* involves a high-affinity membrane-integrated binding protein. J Bacteriol 1999;181:4285–4291.
6. Wanner C, Soppa J. Genetic identification of three ABC transporters as essential elements for nitrate respiration in *Haloferax volcanii*. Genetics 1999;152:1417–1428.
7. Diez J, Diederichs K, Greller G, Horlacher R, Boos W, Welte W. The crystal structure of a liganded trehalose/maltose-binding protein from the hyperthermophilic Archaeon *Thermococcus litoralis* at 1.85 A. J Mol Biol 2001;305:905–915.
8. Lakowicz JR. Principles of fluorescence spectroscopy. 2nd ed. New York: Kluwer Academic/Plenum Publishers; 1999. 698 p.
9. Spurlino JC, Rodseth LE, Quiocho FA. Atomic interactions in protein-carbohydrate complexes. Tryptophan residues in the periplasmic maltodextrin receptor for active transport and chemotaxis. J Mol Biol 1992;226:15–22.
10. Sun YJ, Rose J, Wang BC, Hsiao CD. The structure of glutamine-binding protein complexed with glutamine at 1.94 angstrom resolution: comparisons with other amino acid binding proteins. J Mol Biol 1998;278:219–229.
11. D'Auria S, Lakowicz JR. Enzyme fluorescence as a sensing tool: new perspectives in biotechnology. Curr Opin Biotechnol 2001;12: 99–104.
12. Horlacher R, Xavier KB, Santos H, DiRuggiero J, Kossmann M, Boos W. Archaeal binding protein-dependent ABC transporter: molecular and biochemical analysis of the trehalose/maltose transport system of the hyperthermophilic archaeon *Thermococcus litoralis*. J Bacteriol 1998;180:680–689.
13. Bradford MM. A rapid and sensitive method for the quantitation of microgram quantities of protein utilizing the principle of protein-dye binding. Anal Biochem 1976;72:248–254.
14. Lakowicz JR, Gryczynski I. Frequency-domain fluorescence spectroscopy. In: Lakowicz JR, editor. Topics in fluorescence spectroscopy. Vol 1: Techniques. New York: Plenum Press; 1991. p 293–355.
15. Lehrer SS. Solute perturbation of protein fluorescence. The quenching of the tryptophyl fluorescence of model compounds and of lysozyme by iodide ion. Biochemistry 1971;10:3254–3263.
16. Salomaa P, Schaleger LL, Long FA. Solvent deuterium isotope effects on acid-base equilibria. J Am Chem Soc 1964;86:1–7.
17. Tanfani F, Galeazzi T, Curatola G, Bertoli E, Ferretti G. Reduced beta-strand content in apoprotein B-100 in smaller and denser low-density lipoprotein subclasses as probed by Fourier-transform infrared spectroscopy. Biochem J 1997;322:765–769.
18. Noda I. Generalized two-dimensional correlation method applicable to infrared, Raman, and other types of spectroscopy. Appl Spectrosc 1993;47:1329–1336.
19. Ausili A, Di Lauro B, Cobucci-Ponzano B, et al. Two-dimensional IR correlation spectroscopy of mutants of the beta-glycosidase from the hyperthermophilic archaeon *Sulfolobus solfataricus* identifies the mechanism of quaternary structure stabilization and unravels the sequence of thermal unfolding events. Biochem J 2004;384:69–78.
20. D'Auria S, Scire A, Varriale A,et al. Binding of glutamine to glutamine-binding protein from *Escherichia coli* induces changes in protein structure and increases protein stability. Proteins 2005;58:80–87.
21. Berman HM, Henrick K, Nakamura H. Announcing the worldwide Protein Data Bank. Nat Struct Biol 2003;10:980.
22. Kabsch W, Sander C. Dictionary of protein secondary structure: pattern recognition of hydrogen-bonded and geometrical features. Biopolymers 1983;22:2577–2637.
23. Hubbard SJ, Campbell SF, Thornton JM. Molecular recognition. Conformational analysis of limited proteolytic sites and serine proteinase protein inhibitors. J Mol Biol 1991;220:507–530.
24. McDonald IK, Thornton JM. Satisfying hydrogen bonding potential in proteins. J Mol Biol 1994;238:777–793.
25. Eftink MR. Intrinsic fluorescence of proteins. In: Lakowicz JR, editor. Topics in fluorescence spectroscopy. Vol 6. New York: Kluwer Academic/Plenum Publishers; 2000. p 1–15.
26. D'Auria S, Herman P, Lakowicz JR, et al. The esterase from the thermophilic eubacterium *Bacillus acidocaldariu*s: Structural-functional relationship and comparison with the esterase from the hyperthermophilic archaeon *Archaeoglobus fulgidus*. Proteins 2000;40:473–481.
27. Eftink MR, Ghiron CA. Fluorescence quenching of indole in a model micelle systems. J Phys Chem 1976;80:486–493.
28. Byler DM, Susi H. Examination of the secondary structure of proteins by deconvolved FTIR spectra. Biopolymers 1986;25:469–487.
29. Arrondo JLR, Muga A, Castresana J, Goni FM. Quantitative studies of the structure of proteins in solution by Fourier-transform infrared-spectroscopy. Prog Biophys Mol Biol 1993;59(1): 23–56.
30. Krimm S, Bandekar J. Vibrational spectroscopy and conformation of peptides, polypeptides, and proteins. Adv Protein Chem 1986;38: 181–364.
31. Jackson M, Mantsch HH. Halogenated alcohols as solvents for proteins: FTIR spectroscopic studies. Biochim Biophys Acta 1992; 1118:139–143.
32. Pedone E, Bartolucci S, Rossi M, et al. Structural and thermal stability analysis of *Escherichia coli* and *Alicyclobacillus acidocaldarius* thioredoxin revealed a molten globule-like state in thermal denaturation pathway of the proteins: an infrared spectroscopic study. Biochem J 2003;373(Pt 3):875–883.
33. Barth A. The infrared absorption of amino acid side chains. Prog Biophys Mol Biol 2000;74(3–5):141–173.
34. Barth A, Zscherp C. What vibrations tell us about proteins. Q Rev Biophys 2002;35(4):369–430.
35. Osborne HB, Nabedryk-Viala E. Infrared measurements of peptide hydrogen exchange in rhodopsin. Methods Enzymol 1982;88: 676–680.
36. Banecki B, Zylicz M, Bertoli E, Tanfani F. Structural and functional relationships in DnaK and DnaK756 heat-shock proteins from *Escherichia coli*. J Biol Chem 1992;267:25051–25058.
37. Febbraio F, Andolfo A, Tanfani F, et al. Thermal stability and

aggregation of *Sulfolobus solfataricus* beta-glycosidase are dependent upon the N-epsilon-methylation of specific lysyl residues: critical role of in vivo post-translational modifications. J Biol Chem 2004;279:10185–10194.
38. Lide DR, editor. CRC handbook of chemistry and physics. 84th ed. New York: CRC Press; 2003. 2616 p.
39. Herman P, Vecer J, Barvik I Jr, et al. The role of calcium in the conformational dynamics and thermal stability of the D-galactose/D-glucose-binding protein from *Escherichia coli*. Proteins 2005; 61(1):184–195.
40. Ehrmann M, Ehrle R, Hofmann E, Boos W, Schlosser A. The ABC maltose transporter. Mol Microbiol 1998;29:685–694.
41. Finerty PJ, Muhandiram R, Forman-Kay JD. Side-chain dynamics of the SAP SH2 domain correlate with a binding hot spot and a region with conformational plasticity. J Mol Biol 2002;322:605–620.
42. Forman-Kay JD. The 'dynamics' in the thermodynamics of binding. Nat Struct Biol 1999;6:1086–1087.
43. Obsilova V, Herman P, Vecer J, Sulc M, Teisinger J, Obsil T. 14-3-3zeta C-terminal stretch changes its conformation upon ligand binding and phosphorylation at Thr232. J Biol Chem 2004;279:4531–4540.
44. Yu L, Zhu CX, Tse-Dinh YC, Fesik SW. Backbone dynamics of the C-terminal domain of *Escherichia coli* topoisomerase I in the absence and presence of single-stranded DNA. Biochemistry 1996;35:9661–9666.
45. Zidek L, Novotny MV, Stone MJ. Increased protein backbone conformational entropy upon hydrophobic ligand binding. Nat Struct Biol 1999;6:1118–1121.
46. Chi Y, Kumar TK, Chiu IM, Yu C. 15N NMR relaxation studies of free and ligand-bound human acidic fibroblast growth factor. J Biol Chem 2000;275:39444–39450.